

Control of hybrid standalone power supply system using artificial neural network

Kaushal Prasad Tiwari* , Kishor Thakre 

Department of Electrical and Electronics Engineering, Rabindranath Tagore University, Bhopal, India.

*Corresponding author: tiwarikaushalprasad936@gmail.com

Original Research

Received:
23 December 2024
Revised:
29 January 2025
Accepted:
2 February 2025
Published online:
1 March 2025

© 2025 The Author(s). Published by the OICC Press under the terms of the [Creative Commons Attribution License](https://creativecommons.org/licenses/by/4.0/), which permits use, distribution and reproduction in any medium, provided the original work is properly cited.

Abstract:

Hybrid stand-alone systems are extensively used to supply power in different industries for a wide range of applications. In order to guarantee a steady supply of power to loads despite of variations in load, wind speed, and solar irradiation, these systems need a battery storage system. In standalone power systems, maintaining power quality is essential, particularly in systems that rely on hybrid energy sources. The battery is connected to the network using a bidirectional DC-DC converter with a suitable control mechanism. In this paper, wind turbines and multiple PV are used in parallel and series combinations to ascertain the proper rating of power supply systems. This system uses long short-term memory (LSTM) based artificial neural network (ANN) controllers. The controller for battery has been explicitly designed to guarantee that electricity is distributed equally between the load and the overall generation. Such methods can improve power quality in different areas, such as variations on the supply side from renewable sources and demand-side timescales. The performance analysis using the MATLAB/Simulink platform, and realistic results are generated by implementing Hardware-in-the-Loop through OPAL-RT modules. The results are verified with various case studies to justify the importance of adopted procedure in detail.

Keywords: Wind; Photovoltaic; Maximum power point tracking; Power quality; Hybrid microgrid

1. Introduction

For standalone power supply systems, renewable energy sources are growing in popularity as a way to cut pollution. The system may be more dependable by adding more renewable energy sources. The most efficient method for creating an environmentally friendly system is to use solar and wind power to generate electricity. While wind turbines use the force of the wind to generate mechanical power, photovoltaic (PV) modules convert solar power into electrical energy. In medium power applications, mechanical force is transformed into electrical power using permanent magnet synchronous generators (PMSGs). As a result, standalone power supply systems that combine wind energy and PV have become well-known worldwide. To maintain power equilibrium and give customers consistent power even in the face of variations in solar irradiance, wind speed, and load, standalone systems must incorporate an energy storage system. When coupled, PMSG-based solar and wind power systems can further improve system dependability. Because batteries react quickly throughout the charging and discharging process, they are the best energy storage devices available. To increase system stability and depend-

ability under various operating circumstances, this study recommends using a battery bank. Moreover, a DC-DC bidirectional converter is integrated to efficiently control the battery charging and discharging processes while taking into account the differential power between the generator and the load.

It is essential to use MPPT converters and suitable algorithms to maximize the performance of wind turbines and PV modules [1, 2]. The power generation standalone hybrid system integrates these converters as boost converters so they can function as MPPT converters. To ensure stability between load and power generation, the DC-link is controlled by the DC-DC converter. Power supply to the AC loads is obtained with a suitable controlling mechanism from the DC link. Furthermore, $1 - \emptyset$ loads operated by the distribution system could cause the three-phase terminals' voltages to be unbalanced [3, 4]. Batteries store any extra power that is not needed, so to enable quick charging, the DC-link voltage must be higher than the voltage of the batteries. Similarly, in the event of a power shortage from generation, to accommodate the additional load, the battery bank needs to be depleted. Consequently, when the battery

is being discharged, a boost operation is required. The imbalance of power among the load & generation results in fluctuation of the DC-link voltage [4]. To maintain the equilibrium of power, a DC-DC bidirectional converter is employed, which utilizes the battery to compensate for this difference. The voltage at the AC bus is controlled by the inverter when the DC-link voltage is stable. However, customers continuously demand higher power quality from the source, making it crucial to effectively manage the inverter to ensure a reliable power supply for the load bus. At the PCC, maintaining a stable alternating voltage is very crucial, when faced with unstable loads, dynamic variations in load, and unpredictable variations in irradiance and wind velocity.

Usually, conventional PI controllers face difficulties dealing with abrupt changes in the power system due to their fixed gains. Hence, while developing control strategies for converters utilized in standalone systems, it becomes imperative to use controllers based on Artificial Neural Networks (ANN). However, ANN systems based on long short-term memory can respond to unpredictable signal interference more quickly and with greater responsiveness. To manage the voltages at the alternating bus and DC-link, this research focuses on creating a deep-learning approach to construct ANN LSTM controllers for various converters.

The paper is organized in the following manner: section 2 offers an in-depth explanation of the system. Section 3 delves into the proposed control strategies that make use of ANN LSTM controllers. The results obtained by simulation and HIL are analyzed in section 4. Finally, section 5 concludes the outcomes of the contained work followed by the

Appendix has system parameters.

2. Description of system

A single PV array and wind system cannot provide a consistent voltage for an extended time. PV modules must be connected in parallel and series configurations to guarantee enough power rating and voltage for the PV system. To generate power, the wind turbine is installed with a PMSG, and a diode rectifier is used to convert this DC power. The wind system and a boost converter are coupled to a common DC link via a suitable controlling algorithm. The required power rating determines how many wind systems are needed. The appendix contains the specifications of a PV array and a wind turbine parameter. Each photovoltaic group is furnished with its individual maximum power point tracking system to optimize energy production. To maintain a constant voltage level, the DC-link is connected with the battery bank and a bidirectional converter. By connecting each MPPT converter to the DC-link separately and utilizing its control strategies to utilize most of the energy possibly independent of solar irradiance and wind speed. This collaborative effort allows the converter to maintain DC-link voltage.

The paper emphasizes a four-wire system capable of handling various loads, such as three and single-phase loads with nonlinear characteristics, by utilizing an inverter to transform direct power into alternating for alternating loads, along with a filter positioned between the load bus and inverter. The design of a stand-alone Battery-Wind-PV based system is shown in Fig. 1. Based on earlier research, the filters, PV module, battery, PMSG, and wind turbine have

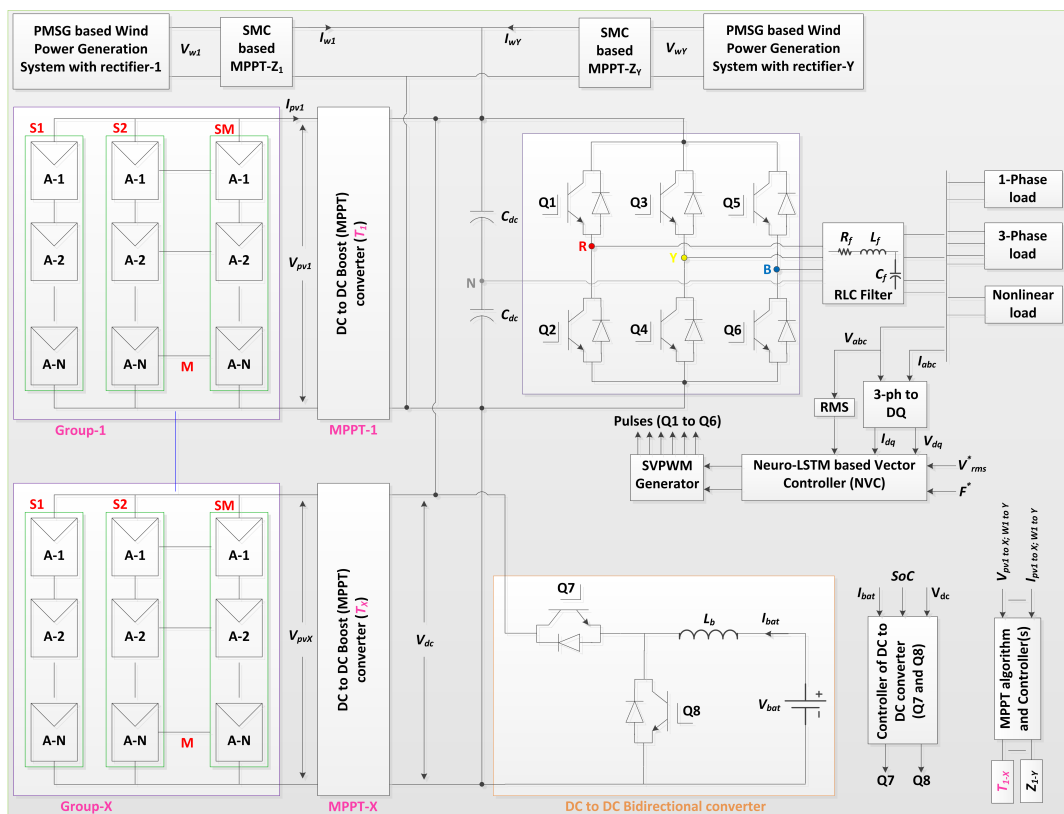


Figure 1. Standalone hybrid power supply system.

been modeled [5–7]. Similar studies have been carried out by several researchers in a variety of settings a few of which are mentioned in the literature. For instance, the authors of [8] used a blend of PV, wind, and batteries to create a stand-alone power supply system. The writers of [9] focused on figuring out where an energy management system would be best placed. In [1] the authors have created a unique MPPT technique for PV systems running in partial shadow. However, [10] proposed a PV-based standalone power system without considering the integration of a wind system. In [5, 11] a TS-Fuzzy-based controller was proposed by the authors for a hybrid Battery-Diesel-PV system. However, including diesel generators in a hybrid structure results in environmental apprehensions. A dual-loop proportional controller specifically intended for the DC-DC converter in a standalone photovoltaic system was proposed in [12]. A comparative analysis of a standalone PV system with nonlinear control is shown in [13], however, the work doesn't include different systems to create a single DC-link or use ANN-LSTM controller. To reduce the harmonics an active power filter is used and PCC for other nonlinear loads. [14]. Moreover, a DSTATCOM is required to counteract the load's requirement for reactive power [15]. Last but not least, a smart grid that combines a variety of renewable energy sources was developed by the authors of [16, 17].

3. Dc-link and inverter voltage control

PV groups experience differences in irradiance, which causes variations in voltage at the MPPT converters' output terminals. In the same way, wind turbines cannot run at the same wind speeds. MPPT converters of boost type may be utilized to make a shared DC-link to address this problem. A P&O-based MPPT is designed for the PV system, while Sliding Mode Control (SMC) based MPPT for wind systems is integrated in this study.

However, due to the fluctuating wind speed, it is not feasible to directly link the output of all the PMSGs. Consequently, the synchronous generator output is transformed to a direct bus through a diode rectifier. Each diode rectifier's output is then linked to the corresponding boost converter, as depicted in Fig. 1. To serve as an MPPT converter for each wind turbine, the boost converter is regulated by an SMC system. Notably, the SMC controller does not require the wind turbine's speed to be sensed. The implemented SMC system is outlined in Fig. 2, with the parameters utilized in the SMC detailed in Table 1. All the boost converters of the wind turbines in the wind farm are connected to a shared DC link, enabling the power generated from all the PMSGs to be injected into the microgrid by elevating the DC link voltage, even during low wind speed conditions. Concurrently, these boost converters can function as MPPT converters for their respective wind turbines by being controlled by the SMC system.

Moreover, the DC-DC converter is essential for controlling the DC link voltage and managing the battery discharging and charging processes. In scenarios where the system experiences swift fluctuations, ANN-based controllers typically exhibit superior performance compared to proportional-integral controllers. Hence, this research paper introduces

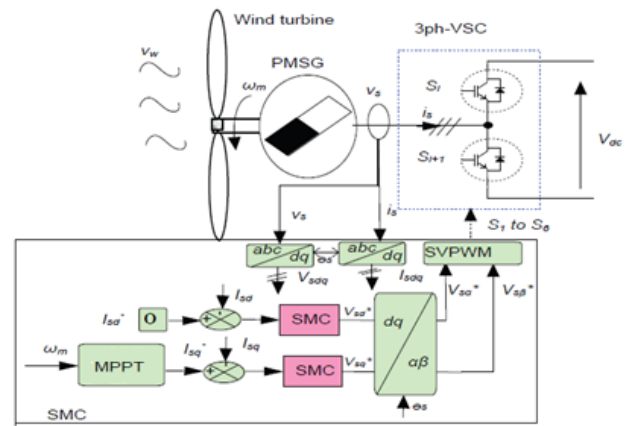


Figure 2. SMC based MPPT of wind turbine.

the aforementioned control scheme to effectively manage grid voltage control at AC and DC buses. Moreover, the ANN controller weights are updated continually by using a deep learning algorithm. Fig. 3 presents the LSTM model, which illustrates the details of the design; Fig. 4 presents the detailed layout of the LSTM-based ANN controller [2, 10, 11].

$$a_t = (w_{ax} \times X_t + w_{ah} \times h_{t-1} + b_a) \sigma \tag{1}$$

$$f_t = (w_{fx} \times X_t + w_{fh} \times h_{t-1} + b_f) \sigma \tag{2}$$

$$O_t = (w_{ox} \times X_t + w_{oh} \times h_{t-1} + b_o) \sigma \tag{3}$$

$$\hat{C}_t = \tanh(w_{cx} \times X_t + w_{ch} \times h_{t-1} + b_c) \tag{4}$$

$$s_t = a_t \times \hat{C}_t + f_t \otimes s_{t-1} \tag{5}$$

$$h_t = O_t \otimes \tanh(s_t) \tag{6}$$

Implementation steps for LSTM algorithm is discussed given below.

Inputs: Data sheet of Energy generation, loads, BESS, and Hydrogen system → Dpp

Output: Predicted Energy Signal

Initialization: considered 'n' number of generation units ← G1, G2, KKGn, 'l' number of loads ← L1, L2, KKLl, etc.

Number of LSTM nodes: NLSTM

1: Procedure LSTM.Prediction

2: Identification for Features from Dpp

3: form ← 0 ton; l; etc

4: Gm[m] ← input1(); Lm[m] ← input2(); etc

5: end for

6: form ← 0 ton; l; etc

7: Normalize G, L and other inputs in range {0, 1}

8: end for

Table 1. SMC parameters.

S. No	Parameter	Value
1	α	298
2	β	0.026
3	δ	0.32
4	ρ	0.012

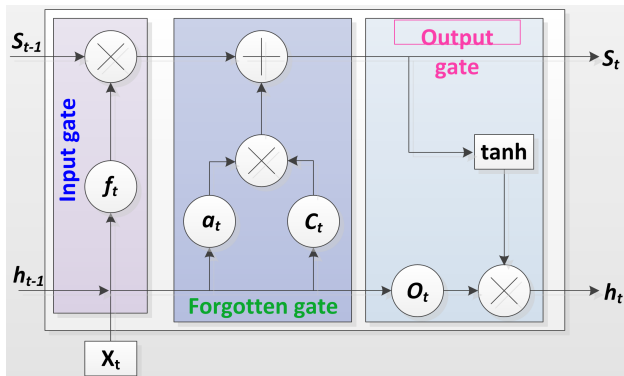


Figure 3. LSTM layout.

```

9: form ← 0 ton; l; etc
10: If {Gm[m]; Lm[m]; etc}. NotValid then
11: inputs ← . Interpolate ()
12: Dpp ← duplicate_value
13: Dp ← processed (Dpp)
14: end if
15: end for
16: Repeat for all LSTM nodes;
17: Output: Predict best_DPP_LSTM_layer_value
18: end procedure
    
```

Nonlinear loads and $1 - \theta$ utilization can introduce oscillations having a frequency of 2ω into the dc-link voltage, which is the main function of the alternating bus. At the connecting terminals of PV panels, these oscillations generate heat and negatively influence the wind turbines by causing shaking. To address the influence of oscillations on the voltage, a proposed solution is to implement a DC-link control method [18, 19]. Using a battery and DC-DC converter, the oscillations are circulated in this manner. Fig. 5 shows the DC-DC converter’s control mechanism.

When there is a discrepancy between the power generated and the power used, the DC link experiences differences. To address this problem a DC-DC converter control strategy has been designed. For the DC-link voltage, this control approach uses a constant reference signal. The battery reference current in Fig. 4 is produced by the proposed controller using the error signal obtained between the references and DC-link voltage. An LPF is used to remove the oscillations, the proposed controller compares to zero, and the oscillating component in the dc-link voltage (i.e., 2ω oscillations) is eliminated. The necessary pulses are generated by comparing the actual battery current with the reference battery current using a hysteresis loop. The 2ω component is circulated more easily through the DC-DC converter

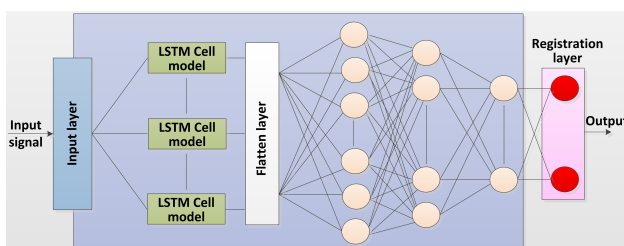


Figure 4. LSTM-ANN model.

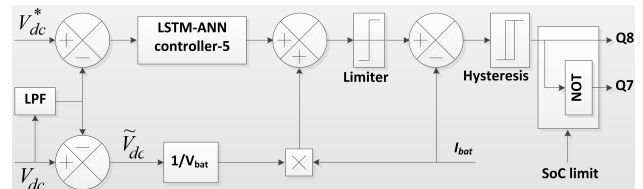


Figure 5. Control scheme for proposed bidirectional circuit.

thanks to this control technique. Additionally, the control scheme design incorporates the state of charge (SOC) to safeguard the battery against overcharging and discharging. An inverter with the right control strategy is necessary for converting DC to AC [16]. After stabilization of DC-link voltage, the voltage output of the inverter may be obtained using MI of the pulse width modulation. Fig. 6 shows the proposed LSTM-ANN controller for the inverter. Maintaining the frequency is essential in a solo system. Significant changes in the active power imbalance may affect the AC output frequency. The reference and frequency error signals are used by the proposed controller to generate the direct axis current’s reference component. Similarly, the reactive component of the current is generated by comparing the reference and RMS voltage. Fig. 6 illustrates how the space vector pulse width modulation (SVPWM) approach generates the appropriate signals for the switches.

4. Results and analysis

MATLAB/Simulink platform is used for the simulation of the proposed work. The HIL is established by utilizing OPAL-RT devices to present diverse reactions under distinct case studies [2]. The OPAL-RT devices and other RTS modules are used in laboratories to achieve HIL configuration. To make the test rig for the proposed complicated controllers in real time, two OPAL-RT 4500 real simulators are used. The plant, which is located in OPAL-RT 1, is made up of PMSG, a wind system, PV, converters, the grid, etc. While all of the controllers are housed in OPAL-RT 2. The plant’s analog signals are converted to digital format using data cards and then input to the OPAL-RT 2. Additionally, this section displays the results of 100 wind systems. The Simulink library’s functional blocks contain all the model’s required parts. The system is constructed in discrete mode, with a sampling time of $20e-6$. Connecting different scopes yields the corresponding outcomes. The model’s achieved findings are listed in the case studies that follow. Fig. 7 illustrates the basic HIL arrangement with two OPAL-RT devices.

4.1 Case-1: performance during changes in load and generation

The unified power of PV is acquired by combining the output power of all PV systems, whereas wind power is the power output of all wind systems taken together. The profile of variations in solar irradiance and wind velocity is shown in Fig. 8. As seen in Fig. 8, the time scale factor employed is 0 seconds, which corresponds to the time at 7 in the morning, and 15 seconds, which corresponds to the time at 10 in the evening. Consequently, the sun irradiance will

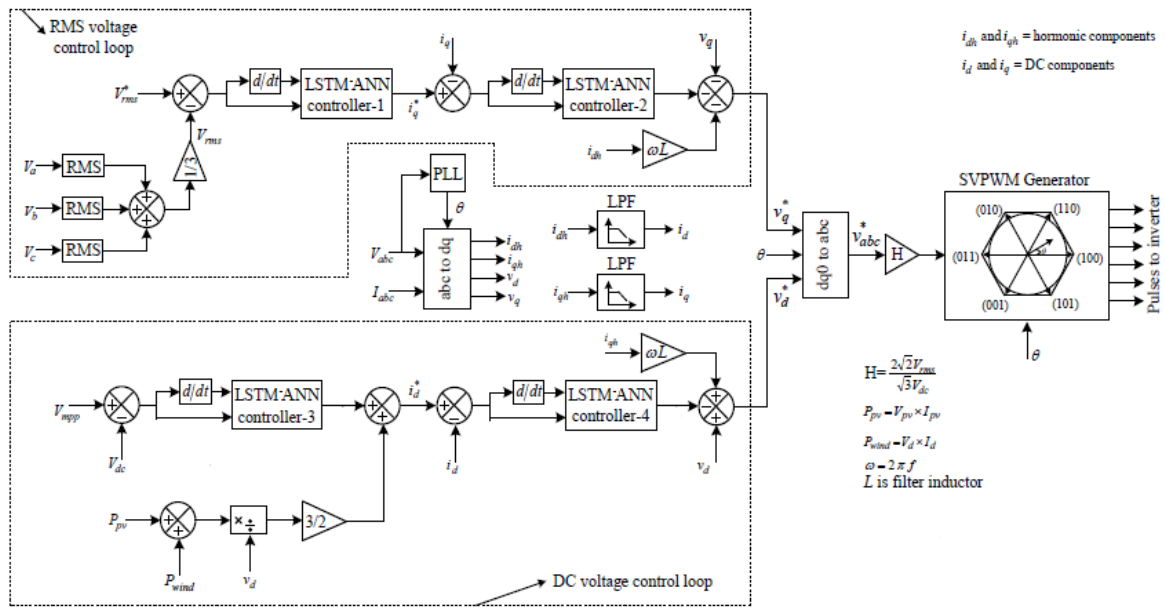


Figure 6. Proposed ANN-LSTM controller for inverter.

peak at 1000 w/m^2 between the hours of 5 and 7 seconds (12 and 2 o'clock).

Like the irradiance, it takes 11 seconds, or 6 PM, for the irradiance to reach its nominal value. The dynamic power production of wind and photovoltaic systems, as well as the variations in power consumption at the alternating bus, are depicted in Fig. 9 (a). The battery bank functions as a stabilizer within the model to ensure equilibrium of n power, making adjustments to compensate for any discrepancies between overall generation and the load. When the battery is discharging to offset the load, it represents positive power, and when it is charging, it indicates negative power. The battery-powered regulated DC-link voltage is depicted in Fig. 9 (b). Even with variations in load power leading to voltage fluctuations at the DC link, these are still negligible when compared to the 720 V reference voltage. The 3-phase system RMS voltages are shown in Fig. 9 (c), demonstrating consistent responses that are attained by applying LSTM-ANN control approaches. For a more practical evaluation of the control methods' effectiveness is verified Opal RT as depicted in Fig. Fig. 9 (d), while, the 3-phase system load currents are depicted in Fig. 10.

4.2 Case-2: smc-mppt of wind turbines

The system has integrated two mass wind turbine models to improve the accuracy of MPPT results. The changes

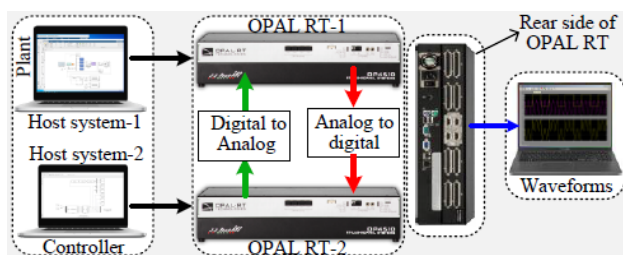


Figure 7. HIL configuration with two OPAL-RT.

in wind speed have been considered, starting at 12 m/s at $t = 1.5 \text{ sec}$, decreasing to 7 m/s, and then increasing again to 10 m/s at $t = 4 \text{ sec}$, as depicted in Fig. 11. The reaction of the wind turbines mechanical torque and reference torque is also shown. It is seen from the waveform that the torque obtained from the wind turbine closely follows the reference torque [8, 9, 20]. The two-mass model's effect is responsible for the torque's steady decline at a rapid fall in wind speed. The wind turbine is operating at its Maximum Power Point (MPP) [9] This is due to the current management of the boost converter, the torque of the PMSG-which is equal to the wind turbine-aligns with the reference torque.

4.3 Case-3: performance during the operation of non-linear and unbalanced load

The PCC is linked to an unbalanced load that draws uneven current, resulting in uneven voltages at the PCC. Other loads connected to the PCC may experience issues as a result of these unequal voltages. Furthermore, the uneven currents drawn by wind farms and solar plant inverters can create 2nd harmonic oscillations, which may potentially harm wind turbine shafts and generate heat on PV arrays. Therefore, it is crucial to maintain balanced voltages at the PCC, even when dealing with unbalanced loads. To pro-

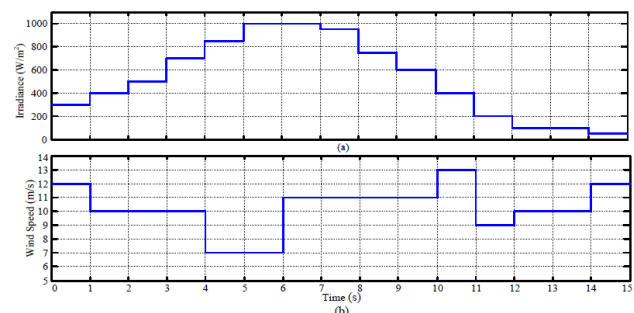


Figure 8. Variations of (a) solar irradiance, (b) wind speed.

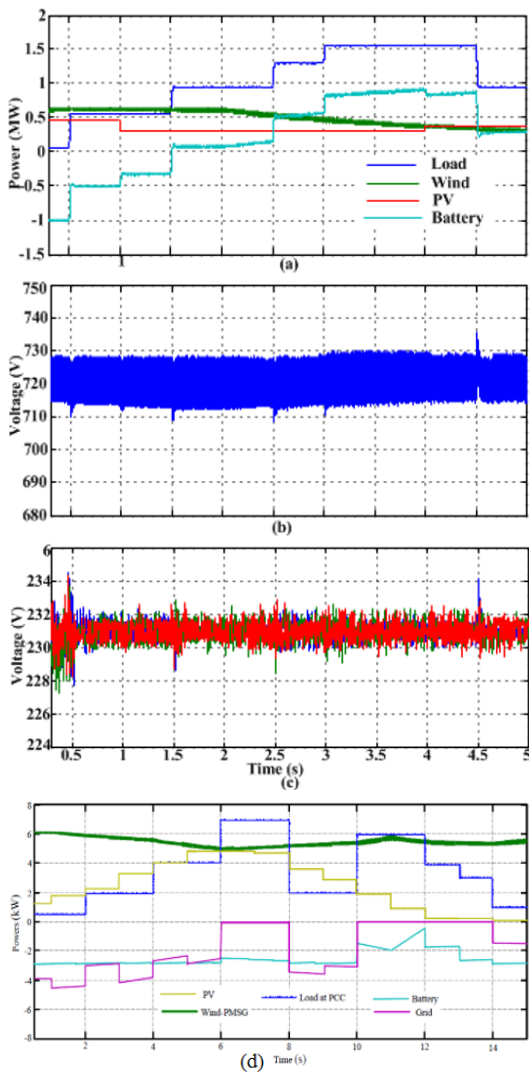


Figure 9. (a) Different Powers, (b) dc-link voltage, (c) RMS phase voltages (d) Opal RT results.

duce uneven currents and maintain balanced PCC voltage, the controller allows oscillations that result from uneven current detection to pass through the electrolyzer-FC inverter. Fig. 12 (a) shows the unbalanced load is supplied at $t = 1.0$ s, and Fig. 12 (b) shows the balanced currents of wind farm-2. The DC-link voltage oscillations of the wind farm are shown in Fig. 12 (c), which also illustrates the inverter’s conventional controller and the suggested controller. The proposed controller successfully eliminates the

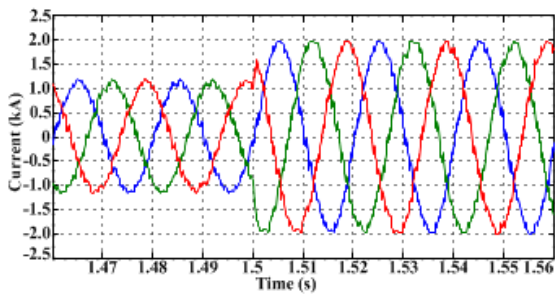


Figure 10. Instantaneous load bus currents.

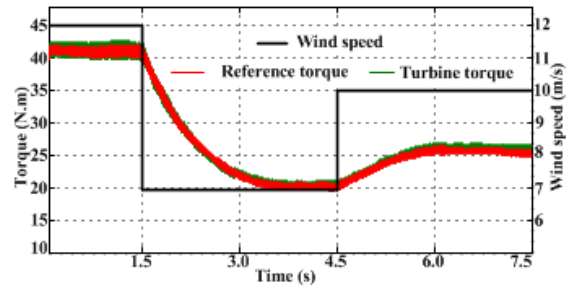


Figure 11. Wind turbine MPPT operation.

2nd harmonic oscillations, as demonstrated in Fig. 12 (d).

4.4 Results under partial shading and uniform irradiance for single module

The findings for power and current at MPP, respectively, displayed at Fig. 13 and Fig. 14 demonstrate how well-correlated and consistent the simulated values are with the measured data.

On the other hand, the agreement between the voltage at MPP and the observed values is worse, and the gradient is often higher than the simulated one as shown in Fig. 15.

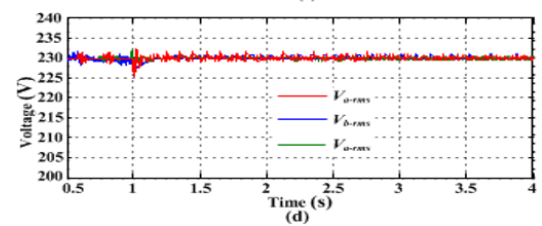
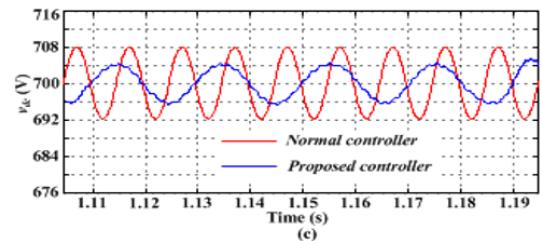
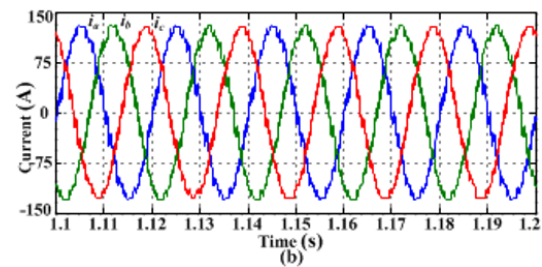
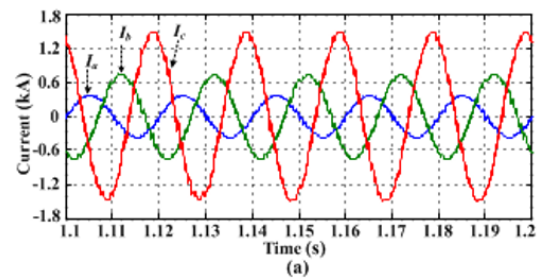


Figure 12. (a) unbalanced load, (b) inverter currents of wind farm-II, (c) DC-link voltage of wind farm-2 inverter, (d) RMS phase voltages at PCC.

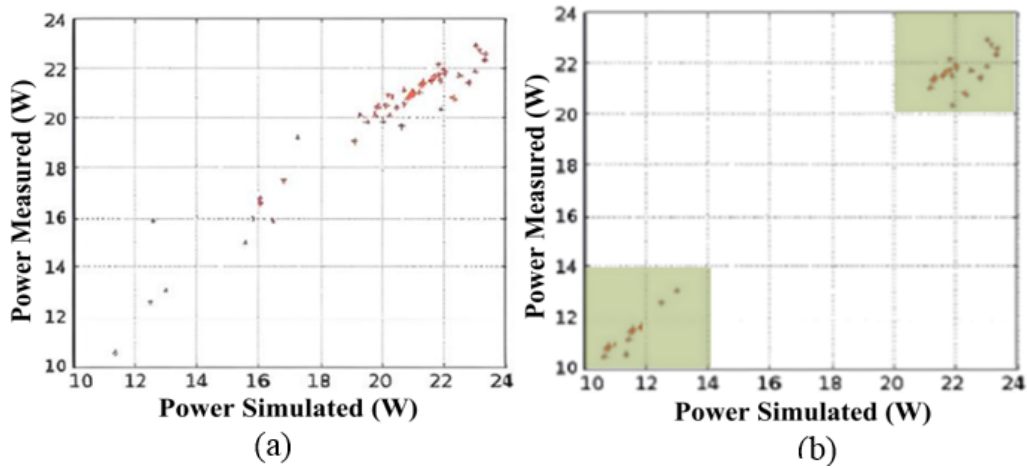


Figure 13. Comparison of simulated and measured power under (a) uniform irradiance (b) partial shading.

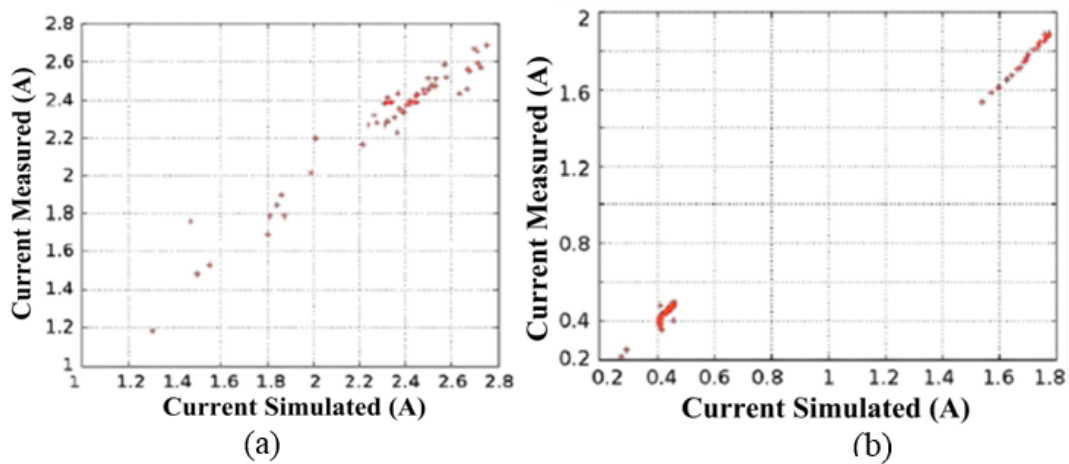


Figure 14. Comparison of simulated and measured current under (a) uniform irradiance (b) partial shading.

5. Conclusion

In the presented work LSTM-based ANN controllers is modeled to regulate the inverter and DC-DC converters in a standalone power supply system powered by hybrid renewable energy sources. An appropriate distribution of power between the overall generation and the load is guaranteed by the specially developed battery controller. The inverter

has a new control strategy to keep the voltage at the AC bus constant even when different factors like wind speed, solar irradiation, and load fluctuations occur. A consistent and reliable power supply is provided at the load bus by seamlessly integrating the battery, PV panels, and wind system. A range of realistic findings are used in the development of Hardware-in-the-Loop using OPAL-RT modules to eval-

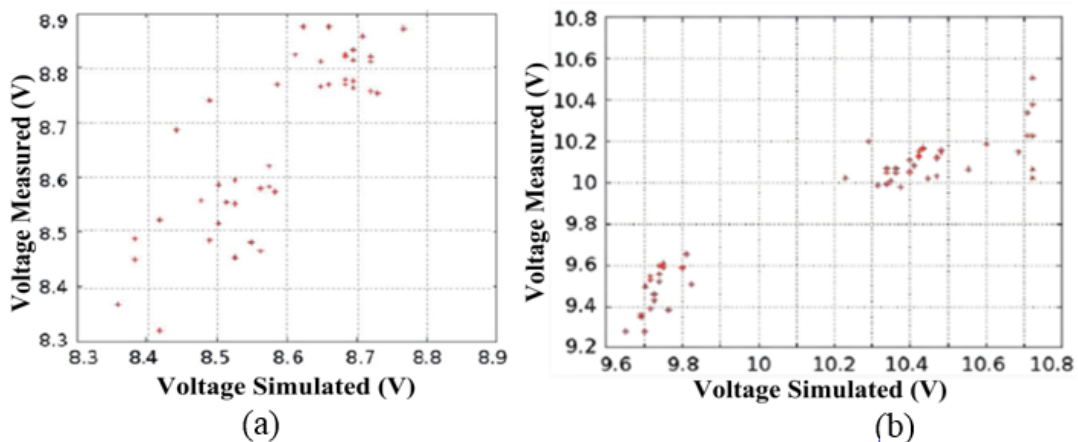


Figure 15. Comparison of simulated and measured voltage under (a) uniform irradiance (b) partial shading.

uate the efficacy of the suggested technique. In the event of unbalanced loads, the suggested inverter management enables the maintenance of balanced 3-phase voltages at the load bus. Moreover, regardless of the current operating conditions, the proposed control techniques greatly improve the power quality.

Authors contributions

Authors have contributed equally in preparing and writing the manuscript.

Availability of data and materials

The data that support the findings of this study are available from the corresponding author upon reasonable request.

Conflict of interests

The authors declare that they have no known competing financial interests or personal relationships that could have appeared to influence the work reported in this paper.

References

- [1] N. Priyadarshi, S. Padmanaban, M. S. Bhaskar, F. Blaabjerg, and A. Sharma. "A fuzzy svpwm based inverter control realization of grid integrated pv-wind system with fpo mppt algorithm for a grid-connected pv/wind power generation system: hardware implementation." *IET Electric Power Appl*, 12(7):962–971, 2018. DOI: <https://doi.org/10.1049/iet-epa.2017.0804>.
- [2] S. G. Malla and C. N. Bhende. "Voltage control of stand-alone wind and solar energy system." *International Journal of Electrical Power & Energy Systems*, 56:361–373, 2014. DOI: <https://doi.org/10.1016/j.ijepes.2013.11.030>.
- [3] C. Pradhan et al. "Coordinated power management and control of standalone pv-hybrid system with modified iwo-based mppt." *IEEE Systems Journal*, 15(3):3585–96, 2021. DOI: <https://doi.org/10.1109/JSYST.2020.3020275>.
- [4] N. Priyadarshi, M. S. Bhaskar, P. Sanjeevikumar, F. Azam, and B. Khan. "High-power dc-dc converter with proposed hsfna mppt for photovoltaic based ultra-fast charging system of electric vehicles." *IET Renewable Power Generation*, 2022. DOI: <https://doi.org/10.1049/rpg2.12513>.
- [5] N. Priyadarshi, P. Sanjeevikumar, M. S. Bhaskar, F. Azam, I. B. Taha, and M. G. Hussien. "An adaptive ts-fuzzy model based rbf neural network learning for grid integrated photovoltaic applications." *IET Renewable Power Generation*, 16(14):3149–3160, 2022. DOI: <https://doi.org/10.1049/rpg2.12505>.
- [6] N. Priyadarshi, S. Padmanaban, M. S. Bhaskar, and B. Khan. "An experimental performance verification of continuous mixed p-norm based adaptive asymmetrical fuzzy logic controller for single stage photovoltaic grid integration." *IET Renewable Power Generation*, 2022. DOI: <https://doi.org/10.1049/rpg2.12410>.
- [7] U. R. Muduli et al. "Cell balancing of li-ion battery pack with adaptive generalised extended state observers for electric vehicle applications." *IEEE Energy Conversion Congress and Exposition (ECCE)*, pages 143–147, 2021. DOI: <https://doi.org/10.1109/ECCE47101.2021.9595601>.
- [8] A. Dash et al. "Dc-offset compensation for three-phase grid-tied spv-dstatcom under partial shading condition with improved pr controller." *IEEE Access*, 9, 2021. DOI: <https://doi.org/10.1109/ACCESS.2021.3115122>.
- [9] H. U. R. Habib et al. "Optimal planning and ems design of pv based standalone rural microgrids." *IEEE Access*, 9, 2021. DOI: <https://doi.org/10.1109/ACCESS.2021.3060031>.
- [10] U. R. Muduli et al. "Predictive battery soc control for dual propulsion differential four wheel drive electric vehicle." *IEEE Energy Conversion Congress and Exposition (ECCE)*, pages 1490–95, 2021. DOI: <https://doi.org/10.1109/ECCE47101.2021.9595587>.
- [11] Jorge Cervantes et al. "Takagi-sugeno dynamic neuro-fuzzy controller of uncertain nonlinear systems." *IEEE Transactions on Fuzzy Systems*, 11(4), 2012. DOI: <https://doi.org/10.1109/TFUZZ.2016.2612697>.
- [12] R. D. Bhagiya and R. M. Patel. "Pwm based double loop pi control of a bidirectional dc-dc converter in a standalone pv/battery dc power system." *IEEE 16th India Council International Conference (INDICON)*, pages 1–4, 2019. DOI: <https://doi.org/10.1109/INDICON47234.2019.9028974>.
- [13] Manisha, M. M. Masoom, and N. Kumar. "Comparative study of nonlinear controllers for standalone pv system." *Second International Conference on Electronics and Sustainable Communication Systems (ICESC)*, pages 25–31, 2021. DOI: <https://doi.org/10.1109/ICESC51422.2021.9532701>.
- [14] U. R. Muduli and K. Ragavan. "Dynamic modeling and control of shunt active power filter." *2014 Eighteenth National Power Systems Conference (NPSC)*, pages 1–6, 2014. DOI: <https://doi.org/10.1109/NPSC.2014.7103893>.
- [15] A. Dash et al. "Performance evaluation of three-phase grid-tied spv-dstatcom with dc-offset compensation under dynamic load condition." *IEEE Access*. DOI: <https://doi.org/10.1109/ACCESS.2021.3132549>.
- [16] V. Narayanan, S. Kewat, and B. Singh. "Solar pv-bes based microgrid system with multifunctional vsc." *IEEE Transactions on Industry Applications*, 56(3):2957–2967, 2020. DOI: <https://doi.org/10.1109/TIA.2020.2979151>.
- [17] X. Song, Y. Zhao, J. Zhou, and Z. Weng. "Reliability varying characteristics of pv-ess-based standalone microgrid." *IEEE Access*, 7:120872–120883, 2019. DOI: <https://doi.org/10.1109/ACCESS.2019.2937623>.
- [18] Koilada Rajesh. "Novel control of boost converter for mppt of wind turbine." *International Journal of New Technologies in Science and Engineering (IJNTSE)*, 8(6):1–6, 2022. DOI: <https://doi.org/10.1016/j.ijhydene.2017.02.028>.
- [19] U. Chaithanya, K. Deepak, D. Besta, M. Khatoon, M. Samyuktha, and P. Mounisha. "A novel control of dc to dc converter for renewable energy sources." *International Conference on Innovative Data Communication Technologies and Application (ICIDCA)*, pages 947–953, 2023. DOI: <https://doi.org/10.1109/ICIDCA56705.2023.10099786>.
- [20] N. Priyadarshi, S. Padmanaban, P. K. Maroti, and A. Sharma. "An extensive practical investigation of fpo-based mppt for grid integrated pv system under variable operating conditions with anti-islanding protection." *IEEE Systems Journal*, 13(2):1861–1871, 2018. DOI: <https://doi.org/10.1109/JSYST.2018.2817584>.

Appendix

Parameters of the proposed module		
S.No	Quantities(s)	Rating
1	Current at V_{mpp} .	7.10 A
2	Voltage at MPP (V_{mpp}).	30.3 V
3	Open-circuit terminal voltage.	36.9 V
4	short-circuit current when	8.01 A
0.5 MW parallel and series combinations		
5	'X' in PV System.	16
6	'M' in Group.	7
7	'N' in String.	21

Two Mass Drive Train

D_t	0.70 p.u.s/el.rads.
K_{sh}	0.30 p.u./el.rads.
H_g	$0.1H_t$.
H_t	4 s

PMSG

Number of poles.	10.0
Rated speed.	153.0 rad/s.
Magnetic flux linkage.	0.433 Wb.
Rated power.	6.4 kW.
Armature resistance (R_s).	0.425 Ω .
Rated torque.	40.0 Nm.
Stator inductance (L_s).	8.4 mH.

Battery Ratings

The proper voltage and power are taken into consideration while determining the battery ratings. This section provides an example using numerical calculations to help make this idea clear. The discharge time is the main factor used to determine the battery rating. In this study, a 480.0 V battery bank is intended to provide backup power for 72.0 hours, enabling a 0.5 MW average load PCC. The given expression is used to approximate the batteries' current rating (Ah), assuming a SoC of 0.6.

$$\text{Current}_{\text{battery}} = \frac{72 \times 5,00,000}{0.6 \times 480} = 125 \text{ kAmp.hr.}$$

Battery parameters of 125 kAh – 400 V system

S.No	Quantities(s)	Rating
1	Strings required in parallel	1000
2	Batteries per string (series).	10.0
3	Current (Single battery)	125 A
4	Voltage (Single battery)	48 V